Heterogeneous Reactions of HX + HONO and I_2 on Ice Surfaces: Kinetics and Linear Correlations

Guowang Diao and Liang T. Chu*

Wadsworth Center, New York State Health Department, and Department of Environmental Health and Toxicology, State University of New York, Albany, New York 12201-0509

Received: September 7, 2004; In Final Form: December 8, 2004

Reaction probabilities of gaseous nitrous acid, HONO, with HCl, HBr, and HI treated ice surfaces have been investigated in a fast flow-tube reactor coupled with a differentially pumped quadrupole mass spectrometer (QMS) at 191 K. The reaction probability increases with the HX surface coverage, and the rate is the highest for the HONO reaction on the HI-treated ice surface. Relative rate constants are correlated to the nucleophilic parameter, according to the linear free-energy relationship for this series of heterogeneous reactions on ice surfaces. The correlation was also extended to $HOCl + HX_{(ad)}$ reactions on the ice surface, and it can be used to treat other heterogeneous atmospheric and catalytic reactions. The reaction products ClNO and BrNO were determined by the QMS. INO was found to rapidly convert to I_2 on surfaces, and I_2 was observed from the reaction of HONO + HI. The uptake coefficient of I_2 on the HI-treated ice surface is higher than that for I_2 on the water−ice surface.

I. Introduction

Heterogeneous reactions play important roles in both manufacturing and natural atmospheric processes. More than half of all chemicals are currently produced via a heterogeneously catalyzed process in which a reaction occurs on the surface of a catalyst.[1] Catalytic cracking of hydrocarbon to produce fuels and the manufacture of integrated circuits via a reaction to deposit films on the surface of a semiconductor are good examples. In the atmosphere, halogen reservoir compounds, $ClONO_2$, are converted to Cl_2 on polar stratospheric cloud surfaces by heterogeneous reactions; this leads to destruction of polar ozone. Progress has been made over the past decade in studying the kinetics and mechanisms of heterogeneous atmospheric reactions such as:

$$ClONO_2 + HCl_{(ad)} \rightarrow Cl_2 + HNO_{3(ad)} \quad (1)$$

$$HOCl + HBr_{(ad)} \rightarrow BrCl + H_2O_{(ad)} \quad (2)$$

$$HOBr + HCl_{(ad)} \rightarrow BrCl + H_2O_{(ad)} \quad (3)$$

An understanding of the occurrence of these reactions on ice surfaces will help to reveal the nature of the polar ozone and boundary-layer ozone loss.[2−11] Reaction 1 is perhaps the most important heterogeneous reaction to convert photochemically inert $ClONO_2$ and HCl into photochemically active chlorine. Because of its significant role in polar ozone depletion, it is the most studied heterogeneous atmospheric reaction. However, even for this reaction, the mechanism of the reaction on ice and acid hydrates still remains controversial. The current understanding of the reaction is that HCl is solvated and perhaps ionized on the ice surface. The nucleophilic attack of Cl^- on the electrophilic chlorine $Cl^{\delta+}$ in solvated $ClONO_2$ molecules is assisted by the ice surface to form Cl_2.[9,12,13] It is uncertain whether the reaction involves an $H_3O^+ \cdot Cl^-$ contact ion pair or a Cl^- ion as the nucleophile, because the barriers for the two pathways are very close, 0.2 kcal/mol, on the basis of quantum calculations.[13] There is a common feature to eqs 1−3: these reactions all involve the ice-catalyzed ionization of hydrogen halides, HX.[14] X^- or contact ion pair attacks the electrophilic $X^{\delta+}$ in $ClONO_2$ or HOX near the ice surface.[15] The rate of the reactions depends on the reactivity of the nucleophile. The nucleophile is a Lewis base in S_N2 reactions in solution. The reactivity increases as the nucleophile decreases in Lewis base hardness. Swain and Scott showed that the relative rate constant increases as the nucleophile varies from Cl^- to Br^- to I^- in solutions, and the relative rate constant can be correlated with structural changes of the reagent using the linear free-energy relationship.[16] The correlation has been successfully used in physical organic chemistry.[17] A similar correlation was applied to the elimination of β-hydride in alkoxides on Cu surfaces, as well as in other catalytic reactions.[18,19] These findings prompted us to study whether there is a linear correlation between the reagent structural change and rate constant in the proton transfer-assisted S_N2 reaction on the ice surface, on the basis of the linear free-energy relationship. Linear free-energy correlation is a powerful tool with which to quantitatively predict the reactivity of other compounds and hard-to-measure rate constants in the series. In this paper, we present the results of kinetics of heterogeneous reactions of

$$HX_{(ad)} + HONO \rightarrow XNO + H_2O_{(ad)} \quad (4)$$

where X = Cl, Br, or I. The reasons why we chose this system were (i) the oxidation state of halides is unchanged during the reaction, (ii) we suggested, in our previous study of the NO_2 + HI reaction,[20] that HI may react heterogeneously with HNO_2, and (iii) reaction 4 may play a role in activating HX on the ice/snow surface in the atmospheric boundary layer.

The heterogeneous reaction of HONO + HBr has been previously studied by our group and others.[21,22] The rate of the

* To whom correspondence should be addressed. E-mail: lchu@albany.edu.

10.1021/jp045965+ CCC: $30.25
Published on Web 01/28/2005

reaction increases slightly as HBr concentration increases. The temperature dependence is weak at $P_{HBr} < 10^{-6}$ Torr, but we note that the reaction probability is higher at 190 K than at 230 K.[21] Chu and co-workers discussed the reaction mechanism using surface kinetics formalism,[21] but did not investigate the effect of reactants (nucleophiles) on the reaction rate. That will be the focus of the present work.

The reaction of HONO + HCl has been studied on the water−ice and frozen HCl solution surfaces at 180−200 K. Fenter and Rossi found that, when initial [HONO] > [HCl], the HONO uptake depended on the amount of HCl adsorbed on the surface, and the rate of the HONO uptake was limited by the amount of HCl on the surface.[23] Product ClNO was observed to be quantitatively proportional to the HONO loss.

In this paper, we provide a brief description of the experimental setup and the measurement of the reaction probability of HONO with HCl, HBr, and HI, at various hydrogen halide concentrations, at 191 K. The results of the reaction probabilities as a function of $[HX_{(ad)}]$, along with the uptake of I_2 on both the HI−ice surface and water−ice surface, are presented. Finally, the effect of nucleophiles on the rate of nucleophilic reactions on ice surfaces is discussed.

II. Experimental Section

2.1. Apparatus. All experiments were performed in a fast flow-tube reactor coupled to a differentially pumped quadrupole mass spectrometer (QMS). The flow-tube and QMS vacuum system were interfaced using a flexible stainless steel bellows and were separated by a valve. Some components of this apparatus have been described in previous papers.[11,24,25] Here, we provide only a brief summary of the major components and modifications of the system.

The double-jacketed cylindrical flow reactor was constructed of Pyrex. Its inner diameter was 1.70 cm, and it was 35 cm in length. The outer jacket was a vacuum layer, to maintain the temperature of the reactor. The temperature of the reactor was regulated by a liquid nitrogen-cooled methanol circulator (Neslab), and was measured with a pair of J-type thermocouples located in the middle and at the downstream end. During the experiment, the temperature was maintained at 191 K; the stability of the temperature was better than 0.2 K in all experiments. The temperature gradient across the flow reactor was approximately 0.3 K. The pressure of the reactor was controlled by a downstream throttle valve (MKS Instruments, Model 651C) and the stability of the pressure was better than 0.002 Torr. The pressure was typically controlled at 0.500 Torr. A double-capillary movable injector was used to admit both HONO and HX into the flow reactor during the reaction-probability measurement. The injector was sealed by a compression fitting with Krytox LVP as lubricant. The lubricant was viscous at low temperature. A heating tape was installed outside of the compression fitting to maintain the temperature at 300 K, so that the injector could be easily pulled out of or pushed in to the reactor.

Reactant HONO vapor was taken from nitrous acid solutions. HONO vapor contains a small amount of water vapor. To avoid condensation of the water vapor and reactants on the capillary wall at a low temperature, we passed room temperature dry air over the outside of the capillary to keep it warm. The flow rate of the reagents was typically less than 10 sccm, while a larger amount of He was mixed with the reagent flow through the flow tube in the laminar-flow condition.

2.2. Reagents. *HX−He Mixtures.* The mixtures of HX−He (X = Cl, Br, or I) were prepared by mixing HX (all from Matheson; HCl 99.999%; HBr 99.8%; HI is a mixture of HI (>99%) and He (99.9995%), 1.08% HI) and ultra-high-purity helium (BOC; 99.9995%) in a glass manifold, which had been previously evacuated to $\sim 10^{-6}$ Torr. The typical HX-to-He mixing ratio was 10^{-2} to 10^{-5}. The HX−He mixture was admitted to the flow reactor via the Pyrex and PFA tubing, and the amount was controlled by a Monel metering valve. The flow rate was determined by monitoring the pressure change in the manifold over time. The calibration of the pressure change versus the flow rate was performed in a separate experiment. All tubing and valves were passivated by the HX−He mixture to establish equilibrium, as monitored by the QMS, prior to each measurement.

I_2−He Mixtures. The I_2−He mixture was prepared by placing a small amount of solid I_2 (Spectrum; I_2 99.8%) in a U-tube, which was immersed in an ice−water bath. I_2 was purified using vacuum. One end of the U-type tube was connected to a 5-L glass bottle via a glass stopcock. The glass bottle was evacuated to 10^{-3} Torr, before the I_2 vapor was diffused into the bottle from the U-tube. After 6 or more h in equilibrium, I_2 pressure in the bottle was equal to its vapor pressure (0.031 Torr at 273.15 K[26]) in the U-tube. Ultra-high-purity helium was then used to fill the bottle to ~600 Torr.

HONO. Gaseous nitrous acid was taken from the vapor phase of the HONO solution. Nitrous acid was prepared by adding drops of H_2SO_4 into a 40-mL 0.2 M $NaNO_2$ solution until a pH of 5.0 was attained at 273.15 K, while the solution was being stirred.[27,28] A clear HONO solution was produced. A higher concentration of HONO can be obtained by increasing the acidity in the solution to pH 4 according to:

$$P_{HONO} = \frac{[NO_2^-]_T}{K_H(1 + K_a/[H^+])} \quad (5)$$

where K_H is the Henry's law constant. K_H was determined to be 218 M/atm at 273.15 K.[21] K_a is the nitrous acid dissociation constant. $[NO_2^-]_T$ is the initial $NaNO_2$ concentration or total N(III) concentration. $[H^+]$ was determined by the pH meter. The nitrous acid solution was prepared fresh frequently during the course of the study, and the solution was kept in the dark at 273 K, both during the experiment and when in storage.

The vapor pressure of nitrous acid for the pH 4 solution at 273 K was measured by an FTIR spectrometer (Mattson, RS-2) using a long path-length cell.[21] The gas-phase nitrous acid concentration was determined based on effective IR cross sections.[29] The sensitivity of the QMS was calibrated to the gas-phase HONO concentration obtained from the FTIR measurement. The estimated accuracy in [HONO] is approximately 20%. The majority of the impurities were NO and NO_2. Fortunately, we found that the loss rates of both NO and NO_2 on ice were insignificant at 191 K.

2.3. Preparation of the Ice Film. Vapor-deposited ice film was prepared as follows. He carrier gas was bubbled through a distilled water reservoir. Deionized water was purified with a Millipore Mili-Q water system. The purified distilled water has a resistivity ≥18 MΩ·cm. The reservoir was maintained at 293.2 ± 0.1 K by a refrigerated circulator (Neslab RTE-100LP). A He−water vapor mixture was admitted to an inlet of the double-capillary injector. During the course of the ice deposition, the double-capillary injector was slowly pulled out at a constant speed, 1.5−2 cm/min, and a uniform ice film was deposited on the inner surface of the flow-tube, which was at 191 K. The amount of ice substrate deposited was determined from the mass

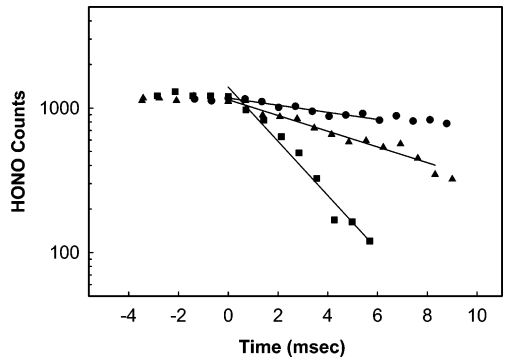

Figure 1. Plot of the HONO signal versus the reaction time (z/v) for a reaction probability experiment. The pseudo-first-order rate constant k_s was determined to be 76.1, 122, and 224 s^{-1} and k_w (see text) was determined to be 79.6, 130, and 256 s^{-1} for HONO with HCl (●), HBr (▲), and HI (■), respectively. γ_w was calculated to be 4.6×10^{-3} for HONO with HCl, 7.5×10^{-3} for HONO with HBr, and 1.5×10^{-2} for HONO with HI. The partial pressure of P_{HX} was 1.5×10^{-5} Torr.

flow rate of the water vapor and the deposition time. The average film thickness was calculated using the measured ice film geometric area, the mass of ice, and the bulk density, 0.63 g/cm^3, of vapor-deposited water−ice.[30] The typical average film thickness was ∼30 μm and the length was ∼25 cm at 191 K. As we had noted in previous studies, the injector and He carrier gases are warmer than the ice film. The He carrier is a potential heating source to warm the ice film. He carrier gas was passed through a cooling coil, which had been placed in dry ice, before admission to the reactor to minimize the heating effect.

2.4. Determination of the Reaction Probability. The reaction probability, γ, is defined as the ratio of the number of molecules that lead to reactions to the total number of molecules colliding with the ice surface. The γ of HONO on the HX-treated ice surface was determined as follows. First, an ice film was vapor deposited on the inner wall of the flow-tube. The film surface was then pretreated with HX at pressures between 10^{-7} and 10^{-5} Torr for approximately 10 min (see below for details). The ice film surface was freshly prepared for every experiment. HONO was then admitted to the reactor via the injector through a separate capillary. The gas-phase HONO concentration was monitored for steadiness by the QMS in order to ensure that all transfer lines (Pyrex and PFA tubing) were passivated prior to every experiment. As the injector was pulled out toward the upstream end of the reactor, 1−2 cm at a time, the gas-phase HONO loss was measured by the QMS at *m*/*e* 47 as a function of the injector position *z*. For a pseudo-first-order reaction under the plug-flow condition, the following equation holds for the reactant HONO:

$$\ln[\mathrm{HONO}]_z = -k_s(z/v) + \ln[\mathrm{HONO}]_0 \qquad (6)$$

where z is the injector position, v is the mean flow velocity, $[\mathrm{HONO}]_z$ is the gas-phase HONO concentration measured by the QMS at position z, and subscript 0 is the initial reference injector position. For a typical experiment performed on HX-treated ice films at 191 K, the pseudo-first-order HONO decay is shown in Figure 1. The pseudo-first-order reaction rate constant, k_s, was determined from the least-squares fit of the experimental data to eq 6. A value of $k_s = 224$ s^{-1} at 191 K was obtained for HI + HONO. k_s was then corrected for gas-phase axial and radial diffusion using a standard procedure,[31] and the corrected rate constant was termed k_w. A diffusion coefficient for HONO in He was estimated to be 467 cm^2·s^{-1}·Torr^{-1} at 191 K and 0.5 Torr.[21,32] The reaction probability γ_w was calculated from k_w using:

$$\gamma_w = 2Rk_w/(\omega + rk_w) \qquad (7)$$

where r is the radius of the flow reactor (0.85 cm) and ω is the mean HONO molecular velocity at 191 K.

It is generally accepted that the vapor-deposited ice film has internal surface areas and is porous. To obtain a reaction probability as if the film is a nonporous surface, γ_w is corrected for contributions from the internal porosity. A common approach is to use a layered pore-diffusion model to obtain the "true" reaction probability, γ_t.[33,34] The ice film is treated as a hexagonally close-packed array of spherical granules stacked in layers.[34] The true reaction probability, γ_t, is related to the value γ_w by

$$\gamma_t = \frac{\sqrt{3}\gamma_w}{\pi\{1 + \eta[2(N_L - 1) + (3/2)^{1/2}]\}} \qquad (8)$$

where the effectiveness factor, η, is the fraction of the film surface that participates in the reaction, and N_L is the number of granule layers. A tortuosity factor $\tau = 4$ and true ice density $\rho_t = 0.925$ g·cm^{-3} were used in the calculation, based on previous reports.[33,34]

2.5. Uptake of HX. The ice film was treated by HX molecules prior to measurement of the reaction probability. Uptake of HX molecules on the ice surface was achieved by pulling the injector toward the upstream end a small step at a time, with an increment of ∼0.5 cm, while HX flowed through a capillary in the injector. HX molecules were taken up by the ice film. Uptake was monitored by the QMS at *m*/*e* 36 for HCl, *m*/*e* 80 for HBr, and *m*/*e* 128 for HI. A nearly uniform HX-adsorbed ice surface was prepared. A typical result is shown in Figure 2. The amount of HX uptake on the ice film can be obtained by integration of the amount of HX taken up by the ice surface. The ice film was not saturated by HX at a given partial pressure as the HX signal (HX flow turned off at $t = 29$ min in Figure 2a and $t = 22$ min in Figure 2b) was not recovered back to the initial level (e.g., $t = 18$ min in Figure 2a).

The uptake amount is the net difference between incoming gaseous molecules and desorbed molecules (Figure 2a). Due to the nature of HCl and the ice−surface interaction, we found that the desorption amount varies with the partial HCl pressure. Even when the gas-phase HCl supply was turned off, desorption could still occur; this is shown at $t > 29$ min in Figure 2a. To maintain the amount of HCl on the ice surface as nearly constant as possible during the reaction probability experiment, we admitted additional HCl, which was equal to the desorbed amount.

Previously, we have demonstrated that HBr forms hydrates (under the steady-state equilibrium) and meta-stable states over the ice surface at 188 K.[35] Similar behavior is expected for other HXs; however, due to the limitation of experiments, we did not determine thermodynamic phases of the surface in this study, except HX uptake amount or surface coverage. This will be discussed further in section 4.1.

III. Results

3.1. HX + HONO Reactions. We found that the reactions between HONO and HX (X = Br, Cl, and I) in the gas phase were slow ($k_s \gg k_{gas}$) under our experimental conditions. A reaction between HONO and HX was observed when these hydrogen halide molecules were adsorbed on the ice film. A

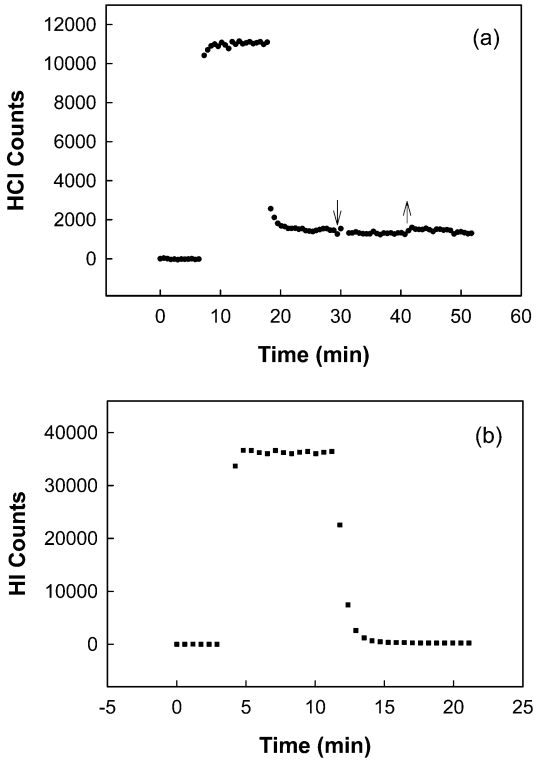

Figure 2. Uptake of HCl and HI on water−ice at 191 K. (a) A plot of the HCl signal. Between times $t = 0$ and 7 min, the background signal was observed. At $t = 7$, the flow of HCl ($P_{HCl} = 3.6 \times 10^{-5}$ Torr) was turned on to ensure a steady HCl signal. Once steady, at $t = 18$ min, the injector was pulled back. Rapid loss of HCl was observed to a value above background. At $t = 29$ min, the HCl flow was turned off (↓), and the signal at $t > 29$ was due to desorption. The injector was pushed back to the downstream end (↑) where there was no ice. (b) A plot of HI signal at $P_{HI} = 6.7 \times 10^{-5}$ Torr. The experimental procedure was similar to that in part a. The injector was pulled back at $t = 12$ min. Rapid loss of HI was observed to a value nearly at the background level. The flow of HI was turned off at $t = 22$ min. We found that desorption of HI from the ice surface can be ignored.

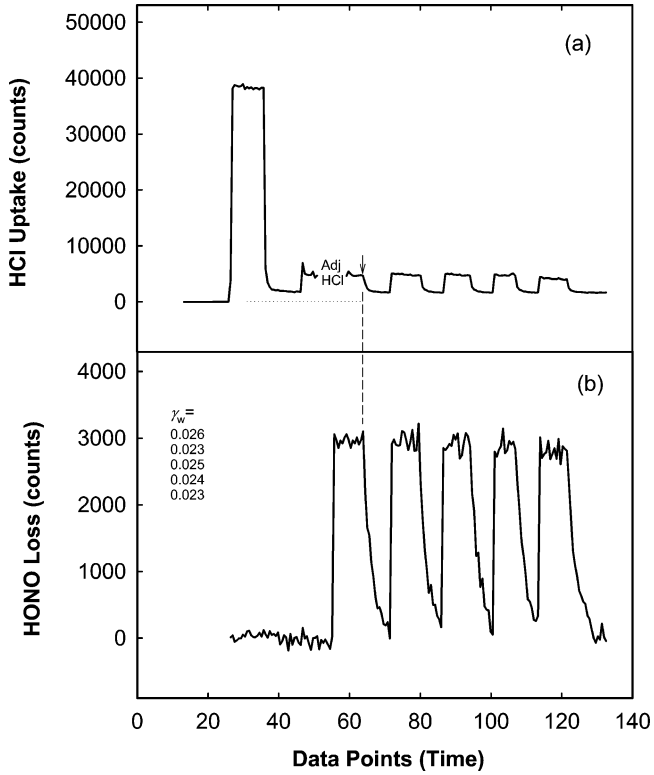

Figure 3. HCl uptake on water−ice and HONO loss on an HCl-treated ice surface. (a) shows a plot of the HCl signal. The background signal was shown at <25 min, and the flow of HCl was turned on at 25 min. Once the HCl signal was steady, the injector was pulled back at 35 min and the rapid loss of HCl on ice was observed. At 46 min, the HCl flow was turned off and the injector was pushed back to the downstream end. The flow of HCl was subsequently readjusted so that the HCl signal level is approximately equal to the desorbed HCl amount. The injector was pulled back again (↓) to measure the loss of HONO on the HCl-treated ice surface, and HCl was taken up by the surface as well. (b) A plot of the HONO signal. The background level of HONO was at <55 min, the HONO flow was turned on at 55 min. The injector was pulled back (indicated by a vertical dashed line) one step at a time and the HONO signal was monitored by QMS (*m*/*e* 47) at different injector positions. The injector was pushed back to the downstream end at 72 min. A new measurement was started at data point = 80 and the procedure was repeated 5 times. Measured values for γ_w were nearly constant when the HCl-treated ice surface was maintained at a constant HCl coverage. The initial reaction probability γ_w was 0.026, and four subsequent measurements yielded $\gamma_w = 0.023$, 0.025, 0.024, and 0.023, respectively.

typical decay of HONO monitored by the QMS as a function of the reaction time is shown in Figure 1. The solid circles represent the change of the HONO signal at *m*/*e* 47 with the reaction time, *t*, when HONO reacted with HCl-treated ice. The open triangles are the loss of HONO over HBr-treated ice, and the squares are the loss of HONO on HI-treated ice. The solid lines are the least-squares fits of the data to eq 6. The slopes of fit are the pseudo-first-order rate constants, k_s, for the reactions of HONO with HCl, HBr, and HI.

A small amount of HCl was observed to desorb from the HCl-adsorbed ice surface continuously at $P_{HCl} > 10^{-6}$ (Figure 2a). The desorbed amount is lower at $P_{HCl} < 10^{-6}$ Torr. The desorption of HBr or HI from the ice surface can be ignored at 191 K (see Figure 2b). Figure 3a (<46 min) shows that the ice film was first doped with HCl to reach a desired coverage. The injector was then pushed back to the downstream end with the HCl flow off. The desorbed amount of HCl was recorded, and additional HCl was supplied to compensate the desorbed HCl. The HCl flow was adjusted so that the HCl signal registered in the QMS was nearly twice the level as the desorbed signal. Once the desired HCl signal level was achieved, the loss of HONO over the HCl treated-ice surface was recorded (Figure 3b, after the dashed line). The procedure was repeated five times on the same surface to illustrate that measurement of γ_w is reproducible: the measured reaction probability, γ_w, was 0.026 (initial γ_w), 0.023, 0.025, 0.024, and 0.023. Within the uncertainty of the measurement (~15%), γ_w is nearly a constant. This suggests that we succcessfully maintained a constant HCl surface coverage.

The reaction probability of HX + HONO was measured as a function of the surface coverage. Note that ice surfaces were not saturated by HX in all experiments. Actual HX surface coverage (uptake amount) was measured in every experiment using the uptake method outlined in section 2.5. The measured rate constants, their corresponding initial reaction probabilities, γ_w and γ_t, and other experimental parameters are listed in Table 1 for the reaction of HCl, HBr, and HI with HONO at 191 K. Most data for k_s, k_w, and γ_w were averaged over 2−3 individual measured values. Errors of ±1 standard deviation, σ, are also included for the measurements in Table 1. The systematic error, estimated to be 7%, was added into the standard deviation. The typical uncertainty in γ_w is approximately 15−30%. The results show that γ_w or γ_t increases as HX coverage increases when [HX] $> 10^{14}$ molecules/cm^2 (Figure 4). The plots show that $\gamma_w^{HI} > \gamma_w^{HBr} > \gamma_w^{HCl}$, where γ_w^{HI}, γ_w^{HBr}, and γ_w^{HCl} are the reaction

TABLE 1: Reaction of HONO with HX-Treated Ice Films

HX	P_{HCl} (Torr)	T (K)	v (ms^{-1})	uptake amt (molecules·cm^{-2})	k_s (s^{-1})	k_w (s^{-1})	γ_w	γ_t
HCl	4.9×10^{-7}	190.9	3.78	1.1×10^{14}	6.4 ± 1.6	6.5 ± 1.7	$(3.8 \pm 1.0) \times 10^{-4}$	7.0×10^{-6}
	8.3×10^{-7}	190.9	3.93	2.2×10^{14}	7.7 ± 2.3	7.8 ± 2.3	$(4.5 \pm 1.4) \times 10^{-4}$	8.5×10^{-6}
	1.4×10^{-6}	190.8	3.95	3.6×10^{14}	4.1 ± 1.4	4.2 ± 1.5	$(2.4 \pm 0.8) \times 10^{-4}$	4.4×10^{-6}
	2.8×10^{-6}	190.8	3.89	6.1×10^{14}	3.1 ± 1.0	3.2 ± 1.1	$(1.7 \pm 0.6) \times 10^{-4}$	3.1×10^{-6}
	4.2×10^{-6}	190.8	3.60	9.9×10^{14}	1.7 ± 0.5	1.7 ± 0.5	$(9.7 \pm 2.6) \times 10^{-5}$	1.7×10^{-6}
	9.3×10^{-6}	190.8	3.74	2.0×10^{15}	3.2 ± 1.9	3.2 ± 1.9	$(1.8 \pm 1.0) \times 10^{-4}$	3.3×10^{-6}
	7.0×10^{-6}	190.8	7.47	2.5×10^{15}	2.3 ± 0.6	2.3 ± 0.6	$(1.3 \pm 0.4) \times 10^{-4}$	2.4×10^{-6}
	1.4×10^{-5}	190.6	7.37	5.2×10^{15}	17.6 ± 5.0	17.8 ± 5.1	$(1.0 \pm 0.3) \times 10^{-3}$	2.2×10^{-5}
	8.2×10^{-6}	190.6	15.4	5.2×10^{15}	38.7 ± 5.8	39.5 ± 6.0	$(2.3 \pm 0.4) \times 10^{-3}$	6.4×10^{-5}
	1.5×10^{-5}	190.4	8.78	6.4×10^{15}	20.1 ± 4.2	20.4 ± 4.3	$(1.2 \pm 0.2) \times 10^{-3}$	2.6×10^{-5}
	1.4×10^{-5}	190.2	14.9	9.8×10^{15}	67.0 ± 29.3	68.8 ± 30.6	$(4.0 \pm 2.8) \times 10^{-3}$	1.6×10^{-4}
	2.7×10^{-5}	190.6	7.26	1.2×10^{16}	40.9 ± 7.2	42.2 ± 8.4	$(2.4 \pm 0.5) \times 10^{-3}$	7.1×10^{-5}
	1.5×10^{-5}	190.5	15.0	1.3×10^{16}	84.1 ± 28.3	88.4 ± 31.1	$(5.1 \pm 1.8) \times 10^{-3}$	2.5×10^{-4}
	3.1×10^{-5}	190.6	14.8	2.7×10^{16}	87.5 ± 30.4	92.3 ± 33.6	$(5.3 \pm 1.9) \times 10^{-3}$	2.7×10^{-4}
	6.6×10^{-5}	190.6	14.5	6.2×10^{16}	218 ± 56	251 ± 73	$(1.4 \pm 0.4) \times 10^{-2}$	1.5×10^{-3}
	1.3×10^{-4}	190.6	15.5	1.4×10^{17}	362 ± 51	448 ± 72	$(2.6 \pm 0.5) \times 10^{-2}$	3.9×10^{-3}

HX	P_{HBr} (Torr)	T (K)	v (ms^{-1})	uptake amt (molecules·cm^{-2})	k_s (s^{-1})	k_w (s^{-1})	γ_w	γ_t
HBr	4.9×10^{-7}	191.2	7.41	2.4×10^{14}	5.4 ± 1.6	5.4 ± 1.7	$(3.1 \pm 1.0) \times 10^{-4}$	5.7×10^{-6}
	8.0×10^{-7}	191.2	7.48	3.8×10^{14}	4.1 ± 1.2	4.1 ± 1.2	$(2.4 \pm 0.7) \times 10^{-4}$	4.3×10^{-6}
	8.7×10^{-7}	190.8	7.08	8.5×10^{14}	6.7 ± 2.0	6.7 ± 2.0	$(3.9 \pm 1.1) \times 10^{-4}$	7.2×10^{-6}
	2.0×10^{-6}	191.5	7.30	9.9×10^{14}	5.6 ± 2.3	5.6 ± 2.4	$(3.2 \pm 1.3) \times 10^{-4}$	5.9×10^{-6}
	3.0×10^{-6}	191.5	7.37	1.5×10^{15}	7.9 ± 2.1	7.9 ± 2.1	$(4.6 \pm 1.3) \times 10^{-4}$	8.6×10^{-6}
	1.7×10^{-6}	190.8	15.5	1.7×10^{15}	16.9 ± 4.2	17.0 ± 4.3	$(9.9 \pm 2.5) \times 10^{-4}$	2.1×10^{-5}
	1.7×10^{-6}	191.2	14.7	1.8×10^{15}	11.2 ± 3.5	11.3 ± 3.5	$(6.6 \pm 2.0) \times 10^{-4}$	1.3×10^{-5}
	3.9×10^{-6}	191.0	7.36	1.9×10^{15}	11.0 ± 3.3	11.2 ± 3.3	$(6.5 \pm 2.0) \times 10^{-4}$	1.3×10^{-5}
	4.8×10^{-6}	191.5	7.22	2.4×10^{15}	32.7 ± 13	34.1 ± 14.3	$(2.0 \pm 0.8) \times 10^{-3}$	5.1×10^{-5}
	4.4×10^{-6}	191.0	14.3	4.5×10^{15}	47.9 ± 21	49.4 ± 22	$(2.9 \pm 1.2) \times 10^{-3}$	9.0×10^{-5}
	5.0×10^{-6}	191.0	14.2	4.8×10^{15}	39.0 ± 5.8	40.0 ± 6.0	$(2.3 \pm 0.4) \times 10^{-3}$	6.5×10^{-5}
	7.8×10^{-6}	190.5	14.2	8.1×10^{15}	73.7 ± 11	77.0 ± 12	$(4.5 \pm 0.8) \times 10^{-3}$	1.9×10^{-4}
	1.5×10^{-5}	190.9	14.4	1.6×10^{16}	118 ± 17	126 ± 18	$(7.3 \pm 1.0) \times 10^{-3}$	4.7×10^{-4}
	1.5×10^{-5}	191.0	15.5	1.6×10^{16}	106 ± 16	113 ± 17	$(6.5 \pm 1.1) \times 10^{-3}$	3.8×10^{-4}
	3.3×10^{-5}	191.0	7.26	1.7×10^{16}	113 ± 17	128 ± 19	$(7.4 \pm 1.1) \times 10^{-3}$	4.8×10^{-4}
	2.4×10^{-5}	191.1	13.9	2.4×10^{16}	150 ± 23	165 ± 25	$(9.5 \pm 1.4) \times 10^{-3}$	7.4×10^{-4}
	2.5×10^{-5}	191.1	15.2	2.7×10^{16}	158 ± 24	173 ± 26	$(1.0 \pm 0.2) \times 10^{-2}$	8.1×10^{-4}
	2.8×10^{-5}	191.1	13.8	2.8×10^{16}	159 ± 14	175 ± 16	$(1.0 \pm 0.2) \times 10^{-2}$	8.2×10^{-4}
	2.9×10^{-5}	191.1	14.6	3.1×10^{16}	182 ± 27	225 ± 34	$(1.3 \pm 0.2) \times 10^{-2}$	1.3×10^{-3}
	3.8×10^{-5}	191.1	15.4	3.9×10^{16}	250 ± 38	289 ± 43	$(1.7 \pm 0.3) \times 10^{-2}$	1.9×10^{-3}
	5.1×10^{-5}	191.1	15.0	5.3×10^{16}	306 ± 45	367 ± 55	$(2.1 \pm 0.3) \times 10^{-2}$	2.8×10^{-3}
	7.1×10^{-5}	190.9	15.1	7.4×10^{16}	370 ± 56	463 ± 69	$(2.6 \pm 0.4) \times 10^{-2}$	4.1×10^{-3}
	7.6×10^{-5}	191.3	14.1	7.8×10^{16}	377 ± 56	478 ± 72	$(2.7 \pm 0.4) \times 10^{-2}$	4.3×10^{-3}

HX	P_{HI} (Torr)	T (K)	v (ms^{-1})	uptake amt (molecules·cm^{-2})	k_s (s^{-1})	k_w (s^{-1})	γ_w	γ_t
HI	8.5×10^{-8}	191.1	3.55	7.4×10^{13}	5.0 ± 1.5	5.1 ± 1.6	$(2.9 \pm 0.9) \times 10^{-4}$	5.3×10^{-6}
	1.3×10^{-7}	191.0	3.61	1.4×10^{14}	5.0 ± 1.5	5.1 ± 1.6	$(3.0 \pm 0.9) \times 10^{-4}$	5.4×10^{-6}
	2.3×10^{-7}	190.9	3.56	2.1×10^{14}	7.4 ± 2.2	7.4 ± 2.2	$(4.3 \pm 1.3) \times 10^{-4}$	8.1×10^{-6}
	2.8×10^{-7}	191.3	3.44	2.6×10^{14}	5.9 ± 1.8	6.0 ± 1.8	$(3.5 \pm 0.9) \times 10^{-4}$	6.3×10^{-6}
	3.5×10^{-6}	191.2	7.12	3.2×10^{14}	6.9 ± 2.0	7.0 ± 2.1	$(4.1 \pm 1.2) \times 10^{-4}$	7.5×10^{-6}
	4.1×10^{-7}	190.8	3.54	4.1×10^{14}	14.2 ± 4.0	14.7 ± 4.2	$(8.5 \pm 2.4) \times 10^{-4}$	1.7×10^{-5}
	5.3×10^{-7}	191.0	3.36	4.8×10^{14}	8.6 ± 2.6	8.8 ± 2.7	$(5.1 \pm 1.5) \times 10^{-4}$	9.7×10^{-6}
	8.0×10^{-7}	190.8	7.04	7.6×10^{14}	13.5 ± 3.7	13.8 ± 3.9	$(8.0 \pm 2.3) \times 10^{-4}$	1.6×10^{-5}
	1.3×10^{-6}	190.9	7.08	1.3×10^{15}	28.4 ± 7.5	29.4 ± 8.0	$(1.7 \pm 0.5) \times 10^{-3}$	4.2×10^{-5}
	1.8×10^{-5}	191.4	14.3	1.7×10^{15}	49.0 ± 6.0	50.5 ± 6.4	$(2.8 \pm 0.5) \times 10^{-3}$	9.0×10^{-5}
	4.0×10^{-6}	191.1	14.5	3.8×10^{15}	64.7 ± 5.1	67.2 ± 5.5	$(3.9 \pm 0.3) \times 10^{-3}$	1.5×10^{-4}
	6.6×10^{-6}	191.1	14.5	6.4×10^{15}	105 ± 12	111 ± 15	$(6.4 \pm 1.0) \times 10^{-3}$	3.7×10^{-4}
	1.1×10^{-5}	191.2	14.5	1.1×10^{16}	134 ± 18	145 ± 21	$(8.4 \pm 1.3) \times 10^{-3}$	5.9×10^{-4}
	1.9×10^{-5}	191.0	14.2	2.0×10^{16}	223 ± 33	255 ± 41	$(1.5 \pm 0.2) \times 10^{-2}$	1.6×10^{-3}
	3.2×10^{-5}	190.9	14.5	3.1×10^{16}	256 ± 40	313 ± 55	$(1.7 \pm 0.2) \times 10^{-2}$	2.0×10^{-3}
	4.2×10^{-5}	191.8	14.3	4.0×10^{16}	326 ± 79	403 ± 113	$(2.3 \pm 0.7) \times 10^{-2}$	3.3×10^{-3}
	6.7×10^{-5}	191.1	15.4	6.6×10^{16}	402 ± 89	523 ± 127	$(3.0 \pm 0.8) \times 10^{-2}$	4.9×10^{-3}

probabilities of HI + HONO, HBr + HONO, and HCl + HONO, respectively. At lower HCl coverage $\sim 10^{14}$ molecules/cm^2, the γ_w value of HONO + HCl increases slightly as [$HCl_{(ad)}$] decreases. It is possible that a change in HCl uptake behavior from submonolayer adsorption to hydrates or amorphous solutions plays a role. This will be discussed in a later section.

3.2. Products. BrNO was observed as a product of the reaction of HONO with HBr-treated ice surface, both in this work and in our previous study.[21] The formation of BrNO was studied in detail previously,[21] and will not be discussed in this paper. We investigated the products of the reaction of HONO with HCl and HI adsorbed on the ice surface thoroughly.

ClNO has several fragments, at *m*/*e* 30, 35, 37, and 49, in the mass spectrum. The QMS signal intensities normalized to *m*/*e* 30 are 0.022 and 0.19, for *m*/*e* 49 and 35, respectively.[23] The peak at *m*/*e* 49 was chosen to monitor the formation of

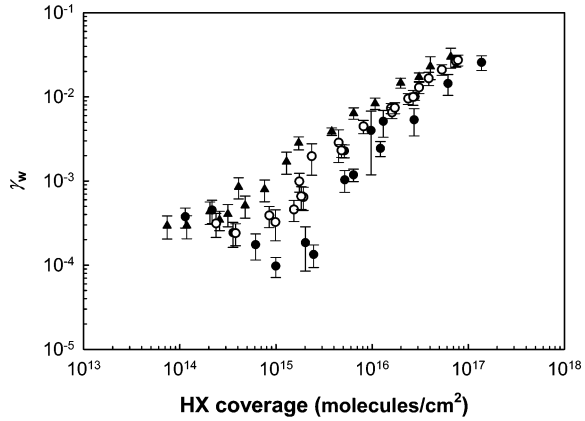

Figure 4. Plot of γ_w as a function of HX surface coverage at 191 K and $P_{HONO} = 1.1 \pm 0.2 \times 10^{-7}$ Torr: (●) HCl + HONO; (○) HBr + HONO; (▲) HI + HONO. γ_w increases as $[HX_{(ad)}]$ increases. Of the three, the reaction probability of HONO + $HI_{(ad)}$ is the highest.

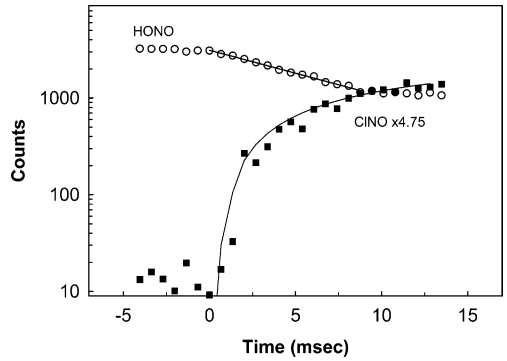

Figure 5. ClNO, monitored by QMS at *m*/*e* 49, was observed in the reaction of HONO + $HCl_{(ad)}$. The pseudo-first-order rate constant was determined to be 76 s^{-1}. The HONO loss rate constant was determined to be 109 s^{-1}.

ClNO, so as to avoid the interference of HCl, NO_2, and NO. We employed higher HONO concentration in product studies to make the detection easier. Figure 5 shows the loss of HONO on the HCl-treated ice surface, and the formation of ClNO. It indicates that ClNO was produced immediately when HONO was lost on the HCl-treated ice surface. The QMS signal of ClNO appears noisy, due to the lower detection sensitivity at *m*/*e* 49. Six experiments were conducted, and k_s values obtained based on the ClNO-formation data were within 35% of the k_s value determined from the HONO loss.

For the reaction of HONO on the HI-treated ice surface, we attempted to determine the formation of INO using the QMS at *m*/*e* 127, 141, and 157. Unfortunately, we were not able to detect INO signal at *m*/*e* 141 and 157, and we did not find the INO signal at *m*/*e* 127 after subtracting out other *m*/*e* 127 components. I_2 was observed at *m*/*e* 254. The formation of I_2 appeared to clearly correlate with the loss of HONO (Figure 6). k_s was determined from the I_2 formation using

$$[I_2]_z = ([I_2]_0 - [I_2]_\infty) \exp(-k_s(z/v)) + [I_2]_\infty \qquad (9)$$

where $[I_2]_\infty$ represents the I_2 concentration in the gas phase at $t = \infty$. The subscripts z and 0 represent the I_2 concentration at the position z and at the reference position 0, respectively. A nonlinear least-squares fitting was used to determine the k_s value, since both $[I_2]_\infty$ and $[I_2]_0$ were treated as constants. The fitted curve is shown in Figure 6 as a solid line. A value for k_s of 391 ± 46 s^{-1} was determined from the I_2 formation; this is in very good agreement with the value of k_s of 370 ± 19 s^{-1}, determined

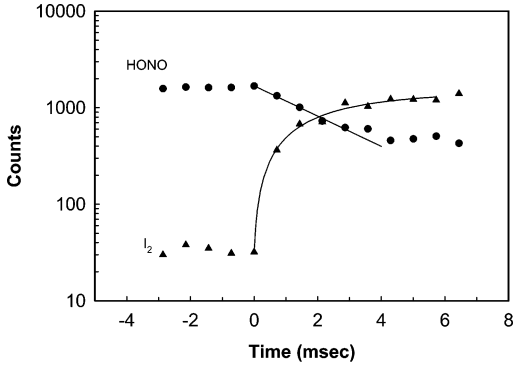

Figure 6. The loss of HONO was monitored by QMS at *m*/*e* 47 on an HI-treated ice film at 193 K. $P_{HONO} = 1.2 \times 10^{-7}$ Torr. $k_s = 370$ s^{-1}, and $\gamma_w = 0.027$. I_2 was measured by the QMS at *m*/*e* 254 during the reaction with $k_s = 391$ s^{-1}. The solid lines are the least-squares fits to the data, using eqs 6 and 9, respectively. See text for details.

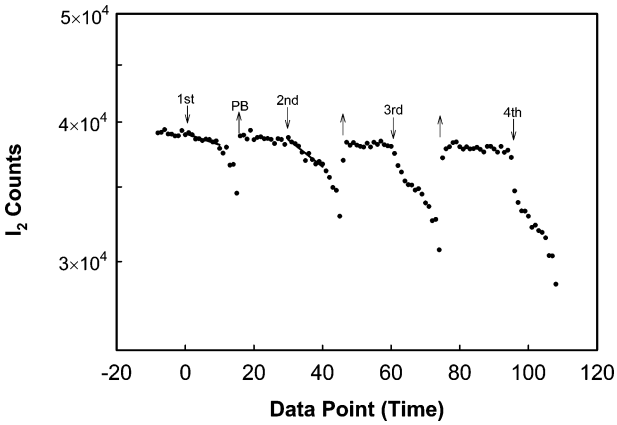

Figure 7. Plot of the I_2 signal versus four consecutive determinations of the uptake coefficient at $P_{I_2} = 1.3 \times 10^{-6}$ Torr and 191.2 K. Each experiment is indicated by an arrow (↓) and the injector was pushed back at the end of an experiment (↑). The initial uptake coefficient was calculated from the slope of plot by using the first measured (1st) data set, as shown by a solid line. The plot shows that the uptake coefficient increases as measurements are repeated. See text for details.

from the loss of HONO. $[HONO]/[I_2]$ was determined to be 0.94 ± 0.3, using the calibrated QMS sensitivity for I_2. We further studied the behavior of I_2 on the water−ice and on the HI-treated ice surface, to reveal the nature of reaction product I_2.

3.3. I_2 on Ice. An I_2−He mixture was admitted to the flow reactor through the movable injector. Prior to exposure of the water−ice surface, transfer lines were passivated by the I_2−He mixture. Figure 7 shows the uptake rate of I_2 on the water−ice surface at 191.1 K and $P_{I_2} = 1.3 \times 10^{-6}$ Torr. The uptake measurement was repeated four times on the same surface. The initial uptake coefficient γ of I_2 on the water−ice surface was 1.5×10^{-4}, and was calculated from the slope using data points recorded in the first experiment, for which the water−ice surface was freshly prepared. By the time the tenth data point was recorded, the uptake rate of I_2 appeared to be increasing with an indication of an increasing slope. This behavior was clearly demonstrated in the second repetition of the experiments. The slope of the plot covering data points 30−40 is less than the slope of the plot covering data points 41−45. The change in uptake behavior may be caused by I_2 multilayer adsorption or dimer formation on the surface. This will be discussed in a later section. The uptake coefficients for the second through fourth repeated measurements are 4.3×10^{-4}, 8.3×10^{-4}, and 1.1×10^{-3}, and they are again higher than the initial uptake coefficient.

TABLE 2: I_2 Uptake Coefficient on HI−Ice Surfaces

P_{I_2} (Torr)	$[HI_{(ad)}]$ (molecules·cm^{-2})	T (K)	k_s (s^{-1})	k_w (s^{-1})	γ
1.1×10^{-6}	5.2×10^{14}	191.6	167 ± 24	189 ± 27	0.025 ± 0.003
1.3×10^{-6}	2.4×10^{15}	191.6	425 ± 36	606 ± 52	0.078 ± 0.01
0.8×10^{-6}	1.3×10^{16}	191.4	441 ± 45	638 ± 67	0.082 ± 0.01

We also conducted an experiment with a reduced data acquisition time (2 s). The initial uptake coefficient was $\gamma = 5.6 \times 10^{-5}$, and γ for the subsequent second through fourth measurements was respectively 1.3×10^{-4}, 2.3×10^{-4}, and 3.6×10^{-4}. This suggests that the I_2 uptake coefficient is affected by the presence of iodine on the surface, and that γ increases as I_2 accumulates on the surface.

3.4. I_2 on HI-Treated Ice. An ice film was treated by HI in the flow reactor. An I_2−He mixture was then admitted to the reactor via the injector, and loss of I_2 on the HI-treated ice surface was observed immediately. A typical result is shown in Figure 8. The figure indicates that the I_2 loss rate on the HI-treated ice surface is very rapid, with $\gamma = 0.072$ at 191.3 K. The initial uptake coefficient γ was measured at several HI surface coverages; the results are listed in Table 2. The study was aimed at the understanding of I_2 from the HONO + HI reaction. However, the γ values at the lower HI coverage should be interpreted with caution. Due to the higher I_2 uptake rate, HI surface coverage may not be high enough; therefore, the measured I_2 uptake coefficient may represent a lower limit at the lowest HI coverage shown in Table 2. The results show that γ is higher at higher HI coverages and that the uptake coefficient of I_2 on HI-treated ice surfaces is higher than the reaction probability of HONO on HI-treated ice surfaces. These facts suggest that if the reaction HONO + $HI_{(ad)}$ produces I_2 directly, I_2 is then adsorbed by the HI-treated ice surface. Clearly, the observed gas-phase I_2 in the HONO + $HI_{(ad)}$ reaction is formed from another pathway.

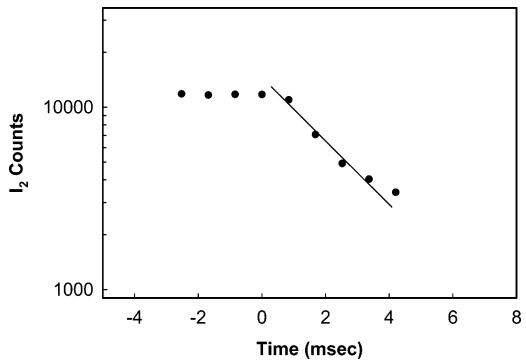

Figure 8. Plot of the I_2 counts versus the uptake time on an HI-treated ice surface. k_s was determined to be 400 s^{-1}. k_w was calculated to be 555 s^{-1}, using the diffusion coefficient of I_2 in He of 345 cm^2·s^{-1}·Torr^{-1}. Initial $\gamma = 0.072$ at 191.3 K and $P_{I_2} = 1.3 \times 10^{-6}$ Torr.

IV. Discussion

4.1. HONO + HX. Figure 4 shows a trend of γ_w increasing as $[HX_{(ad)}]$ increases. However, at lower HX coverage, $<10^{15}$ molecules/cm^2, the γ_w value increases slightly as $[HX_{(ad)}]$ decreases. This is best demonstrated using HONO + $HCl_{(ad)}$ data. γ_w values approach a minimum at $[HCl_{(ad)}] \sim 1 \times 10^{15}$ molecules/cm^2, and then increase slightly as HCl coverage decreases. The explanation for this effect is not completely clear to us. One possibility is that, within the HCl pressure ranges employed for this study, the HCl−ice surface composition falls in "ice" or hydrates phases.[36,37] When $[HCl_{(ad)}] < 10^{15}$ molecules/cm^2, the surface is HCl-doped ice (submonolayer) at 191 K. At higher $[HCl_{(ad)}]$, the surface is either HCl hydrates or amorphous solutions. It is anticipated that the reactivity of HONO toward the HCl-doped ice or hydrate surface is different. It is not necessary to have continuum in reactivity as the surface varies from submonolayer HCl-doped ice to hydrates or solutions. This qualitatively explains the observed discontinuity in γ_w in Figure 4. Further studies are required to quantitatively assess the reactivity of HONO toward HCl in this coverage region. An alternative possibility is that the uncertainty of measurements plays a role, since the error bars of the data are comparable to the variation of γ_w at $[HCl_{(ad)}] \sim 10^{14}$ molecules/cm^2. HCl, HBr, and HI form hydrates near the ice surface at $P_{HX} \sim 10^{-5}$ Torr or higher ($>10^{15}$ molecules/cm^2) under conditions of steady-state adsorption equilibrium.[24,35,36,38,39] The exact HX-ice phase near the ice surface in this study was not investigated and it is not expected to be well defined. However, the coverage was measured and well controlled in every experiment. Regardless of the surface is hydrates, meta-stable states, or amorphous solutions, the higher $[HX_{(ad)}]$ is, the higher the reaction probability γ_w. That was observed in Figure 4. In the rest of the discussion, we assume that the HONO interaction with any HX hydrates or meta-stable phase has a similar reaction pathway at higher HX coverage. Thus, we will concentrate on the data at $[HX_{(ad)}] >$ mid-10^{14} molecules/cm^2.

4.2. Correlation of Rate Constant. Like reaction 1, reaction 4 on the ice surface is a nucleophile-like reaction. Figure 4 shows that the reaction probability increases as the reactant varies in the order from HCl, HBr, and HI. The relative rate constants of many S_N2 organic reactions due to structural changes of the reagent are correlated to the nucleophilic parameter, n, in solution according to the linear free-energy relationship.[16,17] The linear free-energy relationship and the Marcus equation can be used for a group of closely related reactions, and these were applied to catalytic reactions.[1,19] Kraus concluded that it is possible to apply linear correlation parameters obtained in solutions for solid catalyst reactions.[19] We will first identify the rate expression, and then we will correlate the relative rate constant with n.

The experimental observations are consistent with the following Watson reaction steps:

$$HX(g) + S \underset{k_{-10}}{\overset{k_{10}}{\rightleftharpoons}} HX_{(ad)} \qquad (10)$$

where S is the number of ice-surface sites. Quantum chemistry calculations suggest that $HX_{(ad)}$ can be either in contact ion pair or ionization form on the ice surface.[13] Under certain conditions, it may be in the form of HX·nH$_2$O hydrates.[35] However, for the sake of the discussion, we denote it as $HX_{(ad)}$. $HX_{(ad)}$ then reacts with gas-phase HONO through

$$HONO(g) + HX_{(ad)} \underset{k_{-11}}{\overset{k_{11}}{\rightleftharpoons}} HONO\cdots\cdots HX_{(ad)} \xrightarrow{k_2} XNO(g) + H_2O_{(ad)} \qquad (11)$$

Thus, ξ, the rate of the reaction, can be described as

$$\xi = -\frac{d[HONO]}{dt} = k_{11}P_{HONO}[HX_{(ad)}] - k_{-11}[HONO\cdots\cdots HX_{(ad)}] \quad (12)$$

where k_{11} and k_{-11} are respectively the rate constants for the forward and backward reactions of HONO with $HX_{(ad)}$ on the ice surface. k_2 is the rate constant for the decomposition of the intermediate to products. Applying the steady-state approximation to the intermediate, we can write the rate of the reaction as

$$\xi = kP_{HONO}[HX_{(ad)}] \quad (13)$$

where $k = k_{11}k_2/(k_{-11} + k_2)$. γ can be defined as

$$\gamma = \frac{\xi}{\phi_{HONO}} = \frac{\xi\sqrt{2\pi m k_B T}}{P_{HONO}} \quad (14)$$

where ϕ_{HONO} is the flux of HONO impinging on the HX-treated ice surface, m is the molecular weight of HONO, and k_B is the Boltzmann constant. γ can be expressed as

$$\gamma = k\sqrt{2\pi m k_B T}[HX_{(ad)}] \quad (15)$$

Equation 15 shows that γ is proportional to the surface concentration of HX. The higher $[HX_{(ad)}]$ is, the higher the reaction probability. This qualitatively explains the experimental observations presented in Figure 4. A plot of γ versus $[HX_{(ad)}]$ allows us to determine the k value. Several lines of evidence suggest that HX is ionic on the ice surface.[40,41] If we assume that HX is completely ionized on the ice surface, then eqs 10 and 11 would be rewritten to include $H^+_{(ad)}$ and $Cl^-_{(ad)}$. With this modification, we have

$$HONO(g) + X^-_{(ad)} + H^+_{(ad)} \underset{k'_{-11}}{\overset{k'_{11}}{\rightleftharpoons}} HONO\cdots\cdots HX_{(ad)} \xrightarrow{k'_2} XNO(g) + H_2O_{(ad)} + S \quad (16)$$

Equation 15 can be rewritten as

$$\gamma = k\sqrt{2\pi m k_B T}[HX_{(ad)}]^2 \quad (17)$$

recognizing that $[H^+_{(ad)}] = [Cl^-_{(ad)}] = [HX_{(ad)}]$. These are two idealized limits. Realistically, the true reaction probability, γ_t, on a per unit geometric area, may be expressed as

$$\gamma_t = kB[HX_{(ad)}]^p \quad (18)$$

where k is an "overall" rate constant, and $B = \sqrt{2\pi m k_B T}$ and p are constants. The parameter p represents HX adsorption states on the ice surface. Equation 18 forms the basis to determine the rate constants k.

The logarithm of the rate constant, k, is proportional to the standard free energy of activation $\Delta G^{\ddagger}$. A finite change in the standard free energy of the reaction due to a structural change of the reagent may be expressed in terms of $\Delta G^{\ddagger}$ or log k.[17] We can write the relative rate constant in relation to the nucleophilic parameter n as[16,17]

$$\log\frac{k_X}{k_{Cl}} \propto n \quad (19)$$

TABLE 3: Relative Rate Constants and Fitting Parameters for Eq 18

		HONO + $HX_{(ad)}$			HOCl + $HX_{(ad)}$	
X^-	n^a	kB	p	log (k_X/k_{Cl})	kB^b	log (k_X/k_{Cl})
Cl	3.04	1.02×10^{-31}	1.67	0.00	3.41×10^{-7}	0.00
Br	3.89	3.44×10^{-28}	1.48	3.53	1.55×10^{-4}	2.66
I	5.04	2.87×10^{-23}	1.20	8.47		6.25[c]

[a] Value taken from ref 16. [b] Data taken from ref 11 were reanalyzed with eqn 18. [c] Predicted value for the HOCl + HI reaction.

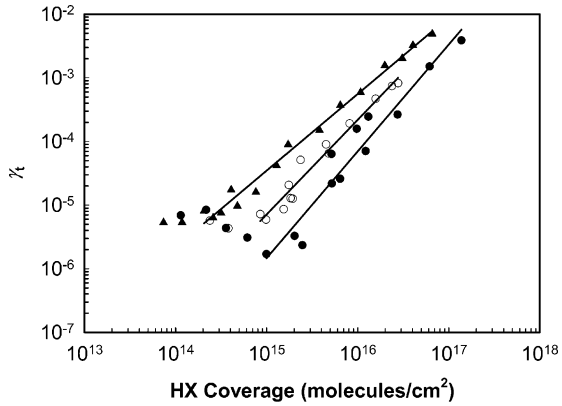

Figure 9. Plot of γ_t versus $[HX_{(ad)}]$: (●) HONO + HCl, (○) HONO + HBr, and (▲) HONO + HI reactions. Solid lines are fitted to eq 18.

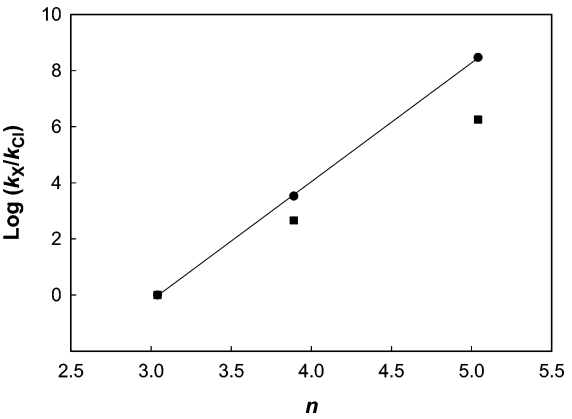

Figure 10. Plot of the relative rate constant log(k_X/k_{Cl}) versus nucleophilic parameter n for a series of HONO + $HX_{(ad)}$ (●) and HOCl + $HX_{(ad)}$ (■) reactions. The plot shows an excellent correlation between the relative rate constant and n. See text for details.

Equation 19 can be expressed in terms of product kB:

$$\log\frac{(kB)_X}{(kB)_{Cl}} = \log\frac{k_X}{k_{Cl}} \propto n \quad (20)$$

Product kB and p in eqn 18 can be determined from the nonlinear least-squares fitting of the data. γ_t in Table 1 was expressed on a per unit geometric surface (nonporous). γ_t values were fitted to eqn 18 to obtain the parameter kB; the result is shown in Figure 9. Data at $[HX_{(ad)}]$ < mid-10^{14} molecules/cm^2 were not included in the fitting, because reactions may follow different pathways, as was discussed in section 4.1. The fitted parameters and the ratio of k_X/k_{Cl} are tabulated in Table 3. A plot of log k_X/k_{Cl} versus n is presented in Figure 10. The correlation coefficient r of the plot is 0.999. Figure 10 clearly shows that the relative rate constant, log(k_X/k_{Cl}), of HX + HONO is correlated to nucleophilic parameters. The excellent correlation suggests that the reaction mechanisms for these three reactions in the series are the same, and that the transition states are similar.

The reaction probability of the HOCl + HBr and HCl was reported as a function of P_{HX} at $10^{-7}-10^{-6}$ Torr and 189 K.[11] Steady-state P_{HX} was converted to the uptake amount using HCl and HBr uptake data,[24,35,42] and the results were reanalyzed using eq 18. The parameter kB is listed in Table 3 as well as the ratio of k_X/k_{Cl}. Log (k_{Br}/k_{Cl}) = 2.66 indicates that the activation of HBr is orders of magnitude faster than that for HCl on a per HX adsorption site basis. The rate constant ratio, k_{Br}/k_{Cl}, was calculated quantum chemically using a three water molecules model.[15] The calculated ratio (4000) is approximately a factor of 8 higher than the experimental value (log (k_{Br}/k_{Cl}) = 2.66). However, the qualitative trend is in agreement. Further, if we apply the linear free-energy relationship to HOCl + HX reactions and if we assume that the functional dependence of γ on coverage or pressure of HI is similar to that for HBr, we can estimate k or γ (Figure 10). The predicted γ is approximately 0.12 at 189 K and $P_{HI} \sim 10^{-7}$ Torr. This correlation approach should be applicable to families of closely related gas−surface reactions on ice surfaces, after it has been validated by further experimental data. The importance of this correlation is that we should be able to quantitatively predict unknown and hard-to-measure rate constants in a series.

4.3. I_2 and the HONO + HI Reaction. Results presented in sections 3.2 and 3.4 show that the γ of I_2 on HI-treated ice is higher than the γ_w of HONO + HI. The stoichiometric ratio [HONO]/[I_2] = 0.94. These facts suggest that I_2 cannot be a direct product of the HONO + $HI_{(ad)}$ reaction. A possible pathway to form I_2 is proposed as follows.

The glass flow tube was interfaced to the QMS vacuum system using a flexible stainless steel bellow and valve. HI may be adsorbed on metal surfaces and atomically dissociated. The dissociation of HI on TiO, Pt, and other surfaces is known to occur without barrier.[43,44] Thus, HI is expected to be dissociatively adsorbed on stainless steel surfaces. The expected product INO reacts with $I_{(ad)}$:

$$INO + I_{(ad)} \rightarrow I_2 + NO \qquad (21)$$

This reaction is feasible for several reasons. (i) The surface coverage of $I_{(ad)}$ is approximately monolayer (10^{14-15} molecules/cm^2), (ii) the gas-phase rate constant for I + INO → I_2 + NO is $k_{I+INO} = 1.66 \times 10^{-10}$ molecules^{-1} cm^3 s^{-1};[45] we anticipate that the corresponding heterogeneous reaction, eq 21, has a comparable rate; (iii) eq 21 satisfies the stoichiometric ratio HONO:INO:I_2 = 1:1:1. The pseudo-first-order rate constant for INO loss can be estimated as $k_{s-21} \approx k_{I+INO}[I_{(ad)}]A/V = 2 \times 10^4$ s^{-1}. This suggests that the reaction is comparable to or faster than HONO + $HI_{(ad)}$. We performed a kinetic simulation at the experimental condition presented in Figure 6 to verify the proposed pathway.[46] The simulation includes reactions 4 and 21−23,[20,45] and k = 370 s^{-1} was used for reaction 4.

$$INO + INO \rightarrow I_2 + 2NO$$
$$k_{23} = 1.3 \times 10^{-14} \text{ molecules}^{-1} \text{ cm}^3 \text{ s}^{-1} \qquad (22)$$

$$NO_2 + HI \rightarrow HNO_2 + I$$
$$k_{24} = 1 \times 10^{-18} \text{ molecules}^{-1} \text{ cm}^3 \text{ s}^{-1} \qquad (23)$$

The results are shown in Figure 11. The simulation suggests that INO was produced from reaction 4, and that nearly all INO were then converted to I_2 via reaction 21. This explains that INO was not detected in our measurement. The analysis of the simulation results suggests that reactions 22 and 23 are too slow to allow formation of I_2. Further, both reactions do not satisfy the observed stoichiometric ratio, HONO:I_2 = 1:1.

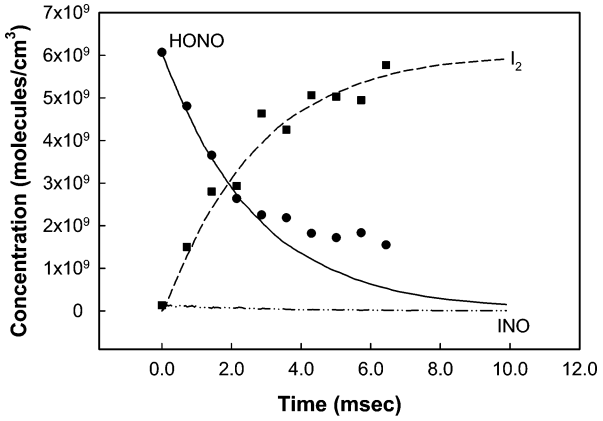

Figure 11. Formation of gas-phase I_2 and INO was simulated by using a kinetic model. The plots suggest that the expected product INO reacted rapidly with $I_{(ad)}$ on surfaces to produce I_2. The lines are derived from the simulation. The simulation agrees well with the experimental observations (I_2, (■); HONO, (●)). See text for details.

4.4. I_2 on Ice. Figure 7 shows that the uptake coefficient of I_2 on the water−ice surface increases as repeated measurements are carried out. The initial uptake coefficient is 1.5×10^{-4}. When the surface was repeatedly exposed to I_2 molecules, I_2, in addition to adsorbing on water−ice surface sites, may adsorb over I_2-covered ice surface sites or may adsorb next to an $I_{2(ad)}$, to form either localized overlayer or islands. This phenomenon is similar to I_2 "dimerization" in solutions.[47] This explains that the uptake coefficient of I_2 from the consecutive measurements is higher than the initial uptake coefficient.

When I_2 is taken up by HI-treated ice surfaces, the uptake coefficient is higher than that for water−ice surfaces. It is likely that the following process plays a role

$$I_2 + I^-_{(ad)} \rightarrow I_3^-{}_{(ad)} \qquad (24)$$

or polyiodide anions on the HI-treated ice surface.

4.5. Comparison with Previous Studies. For the reaction of HONO + $HBr_{(ad)}$ → BrNO + $H_2O_{(ad)}$, we may compare our results to the findings from previous studies. Seisel and Rossi reported that γ_w was $1.7 \times 10^{-4}-1.8 \times 10^{-2}$ under conditions of the concurrent flows of HONO and HBr.[22] γ_w depended on the gas-phase [HBr], tending to reach an upper limit, which is the uptake coefficient of HONO on frozen HBr solutions (2.3×10^{-2}). Chu and co-workers reported that $\gamma_w = 1.3 \times 10^{-3}$ to 1.8×10^{-2} as P_{HBr} varied from 10^{-7} to 10^{-5} Torr at 190 K.[21] The present study shows that $\gamma_w = 2.4 \times 10^{-4}$ to 2.7×10^{-2}. The current γ_w value is slightly lower than the values given in our previous report.[21] The difference is likely due to the fact that γ_w is proportional to [$HBr_{(ad)}$] on the ice surface. The ice surface was nearly saturated by HBr in our previous study; this was not the case in the present study. The γ_w value in the present study is in excellent agreement with the value of Seisel and Rossi.

For the reaction of HONO+$HCl_{(ad)}$ → ClNO+$H_2O_{(ad)}$, Fenter and Rossi found that γ_w is ~4.5×10^{-2} on ice surfaces at 190 K under the HONO and HCl concurrent flow conditions.[23] The HCl flow was $1-4 \times 10^{15}$ molecules/s (3×10^{-5} to 1.2×10^{-4} Torr). Quantitative uptake data were reported on frozen HCl solutions at 190 K. γ_w varied from 6.4×10^{-3} to 1.1×10^{-1} as [HCl] increased from 0.01 to 10 M (corresponding gas-phase flux is $0.9-6 \times 10^{14}$ molecules/s). We found that $\gamma_w \sim 5-25 \times 10^{-3}$ at $P_{HCl} = 2-13 \times 10^{-5}$ Torr conditions. This γ_w

value is lower than that reported by Fenter and Rossi (4.5×10^{-2}); the difference may be due to the differing methods to treat ice surfaces, and the different extents of HCl coverage, in the two studies. It is difficult to compare their results obtained from the frozen solutions directly with ours, mainly because of the difference in surfaces. Comparison of γ_w of the HONO + HI(ad) reaction on the ice surface is not possible, since there are no other reported data for this reaction in the literature.

Allanic and co-workers reported that the uptake coefficient of I_2 on the water−ice surface is below the detection limit of their apparatus ($\gamma < 10^{-3}$).[48] This is in agreement with our observation of a very small uptake coefficient (10^{-4} -10^{-5}). There are no reported data on the value of γ for I_2 on HI−ice surfaces.

V. Conclusions

We have demonstrated that the reaction probability of HONO on HI-treated ice surfaces is higher than that of HONO on HBr-treated ice surfaces, and that the reaction probability of HONO on HBr-treated ice surfaces is higher than that of HONO on HCl-treated ice surfaces. The reaction probability increases with $[HX_{(ad)}]$. The expected reaction products ClNO and BrNO were observed. INO was found to rapidly convert to I_2 on the HI-treated surface. I_2 was observed as a product, and the concentration ratio $[HONO]/[I_2]$ of 0.94 was determined. The relative rate constants of the heterogeneous reactions correlate well with the nucleophilic parameter, *n*, according to the linear free-energy relationship. This correlation may be extended to other series of heterogeneous reactions on ice surfaces, and can be used to predict quantitatively the reactivity of other compounds of a given series. The I_2 uptake coefficient on water−ice is $\gamma \sim 10^{-4}$ and it increases to 0.08 on the HI-treated ice surfaces.

Acknowledgment. The authors thank two anonymous reviewers for helpful suggestions and comments on the manuscript. This work was supported in part by the National Science Foundation, ATM-0355521.

References and Notes

(1) Masel, R. I. *Principles of Adsorption and reaction on solid surfaces*; Wiley: New York, 1996.
(2) Molina, M. J.; Tso, T.; Molina, L. T.; Wang, F. C. Y. *Science* **1987**, *238*, 1253.
(3) Solomon, S.; Garcia, R. R.; Rowland, F. S.; Wuebbles, D. J. *Nature* **1986**, *321*, 755.
(4) Leu, M.-T. *Geophys. Res. Lett.* **1998**, *15*, 17.
(5) Hanson, D. R.; Ravishankara, A. R. *J. Phys. Chem.* **1992**, *96*, 2682.
(6) Chu, L. T.; Leu, M.-T.; Keyser, L. F. *J. Phys. Chem.* **1993**, *97*, 12798.
(7) Abbatt, J. P. D. *Geophys. Res. Lett.* **1994**, *21*, 665.
(8) Oppliger, R.; Allanic, A.; Rossi, M. J. *J. Phys. Chem. A* **1997**, *101*, 1903.
(9) Lee, S.-H.; Leard, D. C.; Zhang, R.; Molina, L. T.; Molina, M. J. *Chem. Phys. Lett.* **1999**, *315*, 7.
(10) Chu, L.; Chu, L. T. *J. Phys. Chem. A* **1999**, *103*, 8640.
(11) Chu, L.; Chu, L. T. *J. Phys. Chem. A* **1999**, *103*, 691.
(12) Bianco, R.; Hynes, J. T. *J. Phys. Chem. A* **1999**, *103*, 3797.
(13) Bianco, R.; Hynes, J. T. *J. Phys. Chem. A* **2003,** *107*, 5253.
(14) Bolton, K.; Pettersson, J. B. C. *J. Am. Chem. Soc.* **2001**, *123*, 7360.
(15) Voegele, A. F.; Tautermann, C. S.; Loerting, T.; Liedl, K. R. *J. Phys. Chem. A* **2002**, *106*, 7850.
(16) Swain, G. G.; Scott, C. B. *J. Am. Chem. Soc.* **1953**, *75*, 141.
(17) Wells, P. R. *Chem. Rev.* **1963**, *67*, 171.
(18) Gellman, A. J.; Dai, Q. *J. Am. Chem. Soc.* **1993**, *115*, 714.
(19) Kraus, M. *Adv. Catal.* **1967**, *17*, 75.
(20) Diao, G.; Chu, L. T. *Phys. Chem. Chem. Phys.* **2001**, *3*, 1622.
(21) Chu, L.; Diao, G. W.; Chu, L. T. *J. Phys. Chem. A* **2000**, *104*, 3150.
(22) Seisel, S.; Rossi, M. J. *Ber. Bunsen-Ges. Phys. Chem.* **1997**, *101*, 943.
(23) Fenter, F. F.; Rossi, M. J. *J. Phys. Chem.* **1996**, *100*, 13765.
(24) Chu, L. T.; Heron, J. W. *Geophys. Res. Lett.* **1995**, *22*, 3211.
(25) Chu, L. T. *J. Vac. Sci. Technol. A* **1997**, *15*, 201.
(26) Dean, J. A. *Lange's Handbook of Chemistry*, 15th ed.; McGraw-Hill: New York, 1999; p 5.33.
(27) Zhang, R.; Leu, M.-T.; Keyser, L. F. *J. Phys. Chem.* **1996**, *100*, 339.
(28) Park, J.-Y.; Lee, U.-N. *J. Phys. Chem.* **1988**, *92*, 6294.
(29) Barney, W. S.; Wingen, L. M.; Lakin, M. J.; Brauers, T.; Stutz, J.; Finlayson-Pitts, B. J. *J. Phys. Chem. A* **2000**, *104*, 1692. Barney, W. S.; Wingen, L. M.; Lakin, M. J.; Brauers, T.; Stutz, J.; Finlayson-Pitts, B. J. *J. Phys. Chem. A* **2001**, *105*, 4166.
(30) Keyser, L. F.; Leu, M.-T. *J. Colloid Interface Sci.* **1993**, *155*, 137.
(31) Brown, R. L. *J. Res. Natl. Bur. Stand.* (*U.S.*) **1978**, *83*, 1.
(32) Cussler, E. L. *Diffusion, mass transfer in fluid systems*; Cambridge University Press: New York,1984; Chapter 5.
(33) Keyser, L. F.; Moore, S. B.; Leu, M.-T. *J. Phys. Chem.* **1991**, *95*, 5496.
(34) Keyser, L. F.; Leu, M.-T.; Moore, S. B. *J. Phys. Chem.* **1993**, *97*, 2800.
(35) Chu, L. T.; Chu, L. *J. Phys. Chem. A* **1999**, *103*, 384.
(36) Hanson, D. R.; Mauersberger, K. *J. Phys. Chem.* **1990**, *94*, 4700.
(37) Abbatt, J. P. D.; Beyer, K. D.; Fucaloro, A. F.; McMahon, J. R.; Wooldridge, P. J.; Zhang, R.; Molina, M. J. *J. Geophys. Res.* **1992**, *97*, 15819.
(38) Chu, L. T.; Chu, L. *J. Phys. Chem. B* **1997**, *101*, 6271.
(39) *Gmelings Handbuch der Anorganicshen Chemie*, No. 8; Verlag Chemie: Berlin, Germany, 1933; pp 293−294
(40) Barone, S. B.; Zondlo, M. A.; Tolbert, M. A. *J. Phys. Chem. A* **1999**, *103*, 9717.
(41) Banham, S. F.; Sodeau, J. R.; Horn, A. B.; McCoustra, M. R. S.; Chesters, M. A. *J. Vac. Sci. Technol. A* **1996**, *14*, 1620.
(42) Chu, L. T.; Leu, M.-T.; Keyser, L. F. *J. Phys. Chem.* **1993**, 97, 7779.
(43) Selloni, A.; Vittadini, A.; Grätzel, M. *Surf. Sci.* **1998**, *402*−*404*, 219.
(44) Taylor, H. S. *Proc. R. Soc. A* **1926**, *113*, 77.
(45) The NIST Chemical Kinetics Database, NIST Standard Reference Database 17-2Q98, Gaithersburg, MD, 1998.
(46) Chemical Kinetics Simulator, Version 1.01, IBM Almaden Research Center, San Jose, CA, 1996, https://www.almaden.ibm.com/st/computational_science/ck/msim/?cks.
(47) Cotton, F. A.; Wilkinson, G. *Advanced Inorganic Chemistry*, 4th ed.; Wiley: New York, 1980; pp 546−547.
(48) Allanic, A.; Oppliger, R.; van den Bergh, H.; Rossi, M. J. *Z. Phys. Chem* **2000**, *214*, 1479.